Biomedical Optics EXPRESS

Optical clearing of archive-compatible paraffin embedded tissue for multiphoton microscopy

Jesse W. Wilson,[1] Simone Degan,[1,2] Warren S. Warren,[1,2,3] and Martin C. Fischer[1,*]

[1]*Department of Chemistry, Duke University, Durham, NC 27708, USA*
[2]*Department of Radiology, Duke University, Durham, NC 27710, USA*
[3]*Department of Biomedical Engineering, Duke University, Durham, NC 27708, USA*
**martin.fischer@duke.edu*

Abstract: Standard histopathology techniques (including paraffin embedding) are incompatible with thick tissue multiphoton imaging, and standard clearing techniques on those specimens destroy some molecular information. We demonstrate multiphoton imaging in specimens prepared according to standard histopathology techniques. This permits unlabeled 3-dimensional histology on archival tissue banks, which is of great value in evaluating prognostic indicators.

OCIS codes: (170.6900) Three-dimensional microscopy; (170.6930) Tissue; (110.0113) Imaging through turbid media.

References and links

1. W. Denk, J. H. Strickler, and W. W. Webb, "Two-photon laser scanning fluorescence microscopy," Science **248**(4951), 73–76 (1990).
2. W. R. Zipfel, R. M. Williams, and W. W. Webb, "Nonlinear magic: multiphoton microscopy in the biosciences," Nat. Biotechnol. **21**(11), 1369–1377 (2003).
3. W. Min, C. W. Freudiger, S. Lu, and X. S. Xie, "Coherent nonlinear optical imaging: beyond fluorescence microscopy," Annu. Rev. Phys. Chem. **62**(1), 507–530 (2011).
4. P. J. Campagnola, A. C. Millard, M. Terasaki, P. E. Hoppe, C. J. Malone, and W. A. Mohler, "Three-dimensional high-resolution second-harmonic generation imaging of endogenous structural proteins in biological tissues," Biophys. J. **82**(1), 493–508 (2002).
5. T. E. Matthews, I. R. Piletic, M. A. Selim, M. J. Simpson, and W. S. Warren, "Pump-probe imaging differentiates melanoma from melanocytic nevi," Sci. Transl. Med. **3**(71), 71ra15 (2011).
6. A. C. Kwan, K. Duff, G. K. Gouras, and W. W. Webb, "Optical visualization of Alzheimer's pathology via multiphoton-excited intrinsic fluorescence and second harmonic generation," Opt. Express **17**(5), 3679–3689 (2009).
7. P. Theer and W. Denk, "On the fundamental imaging-depth limit in two-photon microscopy," J. Opt. Soc. Am. A **23**(12), 3139–3149 (2006).
8. H. Hama, H. Kurokawa, H. Kawano, R. Ando, T. Shimogori, H. Noda, K. Fukami, A. Sakaue-Sawano, and A. Miyawaki, "Scale: a chemical approach for fluorescence imaging and reconstruction of transparent mouse brain," Nat. Neurosci. **14**(11), 1481–1488 (2011).
9. H.-U. Dodt, U. Leischner, A. Schierloh, N. Jährling, C. P. Mauch, K. Deininger, J. M. Deussing, M. Eder, W. Zieglgänsberger, and K. Becker, "Ultramicroscopy: three-dimensional visualization of neuronal networks in the whole mouse brain," Nat. Methods **4**(4), 331–336 (2007).
10. M. A. Smith, E. L. Barnes, and S. I. Chiosea, "Pathology archive: evaluation of integrity, regulatory compliance, and construction of searchable database from print reports," Am. J. Clin. Pathol. **135**(5), 753–759 (2011).
11. J. E. Gershenwald, M. I. Colome, J. E. Lee, P. F. Mansfield, C. Tseng, J. J. Lee, C. M. Balch, and M. I. Ross, "Patterns of recurrence following a negative sentinel lymph node biopsy in 243 patients with stage I or II melanoma," J. Clin. Oncol. **16**(6), 2253–2260 (1998).
12. V. V. Tuchin, "Optical clearing of tissues and blood using the immersion method," J. Phys. D Appl. Phys. **38**(15), 2497–2518 (2005).
13. E. A. Genina, A. N. Bashkatov, and V. V. Tuchin, "Tissue optical immersion clearing," Expert Rev. Med. Devices **7**(6), 825–842 (2010).
14. S. G. Parra, T. H. Chia, J. P. Zinter, and M. J. Levene, "Multiphoton microscopy of cleared mouse organs," J. Biomed. Opt. **15**(3), 036017 (2010).
15. A.-S. Chiang, "Aqueous tissue clearing solution," U.S. patent 6472216 (October 29, 2002).
16. A. J. Lea, "Solubility of melanins," Nature **170**(4330), 709 (1952).
17. T. M. Cooper, S. T. Schuschereba, R. D. O'Connor, D. L. Bolton, and D. L. Lund, *Melanin: The Effects of Dimethyl Sulfoxide on the Spectral Properties* (National Technical Information Service, 1986).

#174845 - $15.00 USD Received 23 Aug 2012; revised 28 Sep 2012; accepted 1 Oct 2012; published 3 Oct 2012

18. N. Sudheendran, M. Mohamed, M. G. Ghosn, V. V. Tuchin, and K. V. Larin, "Assessment of tissue optical clearing as a function of glucose concentration using optical coherence tomography," J. Innov. Opt. Health Sci. **03**(3), 169–176 (2010).
19. J. Wang, Y. Liang, S. Zhang, Y. Zhou, H. Ni, and Y. Li, "Evaluation of optical clearing with the combined liquid paraffin and glycerol mixture," Biomed. Opt. Express **2**(8), 2329–2338 (2011).
20. R. J. Buesa, "Mineral oil: the best xylene substitute for tissue processing yet?" J. Histotechnol. **23**(2), 143–149 (2000).
21. J. Lin, S. H. Kennedy, T. Svarovsky, J. Rogers, J. W. Kemnitz, A. Xu, and K. T. Zondervan, "High-quality genomic DNA extraction from formalin-fixed and paraffin-embedded samples deparaffinized using mineral oil," Anal. Biochem. **395**(2), 265–267 (2009).
22. S. V. Plotnikov, A. C. Millard, P. J. Campagnola, and W. A. Mohler, "Characterization of the myosin-based source for second-harmonic generation from muscle sarcomeres," Biophys. J. **90**(2), 693–703 (2006).
23. R. M. Zucker, "Whole insect and mammalian embryo imaging with confocal microscopy: morphology and apoptosis," Cytometry A **69A**(11), 1143–1152 (2006).
24. T. E. Matthews, J. W. Wilson, S. Degan, M. J. Simpson, J. Y. Jin, J. Y. Zhang, and W. S. Warren, "In vivo and ex vivo epi-mode pump-probe imaging of melanin and microvasculature," Biomed. Opt. Express **2**(6), 1576–1583 (2011).
25. J. W. Wilson, S. Degan, T. Mitropoulos, M. A. Selim, J. Y. Zhang, and W. S. Warren, "In vivo pump-probe microscopy of melanoma and pigmented lesions," Proc. SPIE **8226**, 822602, 822602-8 (2012).
26. V. Williams and F. Morriss, "Formaldehyde-induced fluorescence as a means for differentiating epinephrine cells from norepinephrine cells in adrenal medulla," Stain Technol. **45**(5), 205–213 (1970).
27. U. Leischner, A. Schierloh, W. Zieglgänsberger, and H.-U. Dodt, "Formalin-induced fluorescence reveals cell shape and morphology in biological tissue samples," PLoS ONE **5**(4), e10391 (2010).
28. S. D. Russell and C. P. Daghlian, "Scanning electron microscopic observations on deembedded biological tissue sections: comparison of different fixatives and embedding materials," J. Electron Microsc. Tech. **2**(5), 489–495 (1985).
29. A. T. Yeh, B. Choi, J. S. Nelson, and B. J. Tromberg, "Reversible dissociation of collagen in tissues," J. Invest. Dermatol. **121**(6), 1332–1335 (2003).
30. D. Fu, T. Ye, T. E. Matthews, G. Yurtsever, and W. S. Warren, "Two-color, two-photon, and excited-state absorption microscopy," J. Biomed. Opt. **12**(5), 054004 (2007).
31. O. Katz, E. Small, Y. Bromberg, and Y. Silberberg, "Focusing and compression of ultrashort pulses through scattering media," Nat. Photonics **5**(6), 372–377 (2011).
32. K. Isobe, H. Kawano, T. Takeda, A. Suda, A. Kumagai, H. Mizuno, A. Miyawaki, and K. Midorikawa, "Background-free deep imaging by spatial overlap modulation nonlinear optical microscopy," Biomed. Opt. Express **3**(7), 1594–1608 (2012).
33. D. Kobat, M. E. Durst, N. Nishimura, A. W. Wong, C. B. Schaffer, and C. Xu, "Deep tissue multiphoton microscopy using longer wavelength excitation," Opt. Express **17**(16), 13354–13364 (2009).
34. C.-K. Sun, C.-C. Chen, S.-W. Chu, T.-H. Tsai, Y.-C. Chen, and B.-L. Lin, "Multiharmonic-generation biopsy of skin," Opt. Lett. **28**(24), 2488–2490 (2003).
35. P. Mahou, N. Olivier, G. Labroille, L. Duloquin, J.-M. Sintes, N. Peyriéras, R. Legouis, D. Débarre, and E. Beaurepaire, "Combined third-harmonic generation and four-wave mixing microscopy of tissues and embryos," Biomed. Opt. Express **2**(10), 2837–2849 (2011).
36. P. Samineni, B. Li, J. W. Wilson, W. S. Warren, and M. C. Fischer, "Cross-phase modulation imaging," Opt. Lett. **37**(5), 800–802 (2012).
37. J. W. Wilson, P. Samineni, W. S. Warren, and M. C. Fischer, "Cross-phase modulation spectral shifting: nonlinear phase contrast in a pump-probe microscope," Biomed. Opt. Express **3**(5), 854–862 (2012).

1. Introduction

Multiphoton laser scanning microscopy enables 3-dimensional (3D), high-resolution imaging in thick tissue samples and in vivo [1,2]. Though initially demonstrated with two-photon fluorescence, multiphoton techniques accessing a broad range of label-free, molecule-specific, contrasts are being developed at an exciting pace [3]. These techniques could greatly aid pathologists by providing label-free structural and molecular contrast—they can directly visualize 3D tissue architecture (see for example [4]) and extract chemical information from pathology specimens, such as identifying differences in pigmentation chemistry between melanoma and 'pre-cancerous' dysplastic nevi [5] or localizing senile plaques in Alzheimer's disease via autofluorescence [6]. However, the application of multiphoton techniques to routinely-prepared paraffin-embedded pathology specimens has been limited by optical scattering [7] to thin tissue sections (~5 μm). Though various optical clearing methods have been extraordinarily successful with fresh and fixed tissue [8,9], these techniques either use harsh chemicals (for example, they would dissolve melanin) or are incompatible with prior paraffin embedding. Here, we investigate a more gentle clearing protocol, in which a mixture

#174845 - $15.00 USD Received 23 Aug 2012; revised 28 Sep 2012; accepted 1 Oct 2012; published 3 Oct 2012

of mineral oil and glycerol is found to enable 3D multiphoton histology in paraffin-embedded tissue specimens.

Pathology specimens (such as biopsies) are normally prepared by fixing the tissue in formalin, embedding it in paraffin wax, mechanically sectioning the block to make slides, and archiving the remainder of the block. These archives of human tissue can be extremely valuable in epidemiologic studies [10] or for re-evaluating old cases with newer, more accurate diagnostic methods. For example, investigations into recurrences of melanoma in patients with negative sentinel lymph node biopsies revealed that the standard procedure at the time failed to detect 'occult' metastases that were found upon a painstaking re-evaluation by serial sectioning [11]. Of course, preparing and viewing a series of 5 μm sections through an entire lymph node is laborious, time-consuming, and poses challenges for accurate volume reconstruction. Investigating successive thick sections (several hundred micrometers) could be much more efficient, but the paraffin scattering prevents imaging in sections thicker than a few microns.

The solution we demonstrate here is to deparaffinize the blocks and replace the solvent with a suitable fluid for imaging (the commonly used solvent xylene is volatile and toxic). Various optical clearing protocols have been developed to match the optical index of the tissue components to the fluid medium [12,13]. The most impressive of these are Sca*l*e [8], benzyl alcohol-benzyl benzoate (BABB) [9,14], and FocusClear [15]. However, Sca*l*e is very sensitive to tissue preparation procedures, making it incompatible with previously paraffinized tissue, and benzyl alcohol in BABB and the DMSO in FocusClear are known to dissolve melanin [16,17], making them unsuitable for pigmented specimens.

A number of more gentle clearing agents have been well-characterized and reviewed, including glycerol, glycol, polyethylene glycol, propylene glycol, etc [12]. Of particular interest in clearing deparaffinized specimens is the combination of mineral oil (which is essentially liquid paraffin) and glycerol. Though mineral oil alone has not been observed to induce optical clearing [18], its mixture with glycerol enhances penetration, and has been shown to improve imaging depth in OCT in vivo [19]. (Mineral oil itself has even been used as a deparaffinization agent in preparing histology slides [20,21].) Here we show that the perfusion of thick, deparaffinized tissue with a mixture of mineral oil and glycerol restores multiphoton imaging depth to that achievable in non-paraffinized specimens. We demonstrate this with the two most common multiphoton techniques, autofluorescence and second harmonic generation, and investigate the scattering properties of these cleared specimens.

2. Methods

Freshly excised mouse organs (kidney, liver, spleen, heart, lung, brain, and skin from 12 week old BALB/c mice) were prepared by two methods for comparison—non-paraffinized (NP) and paraffinized-deparaffinized (DP)—both according to standard histology procedures up until the immersion in the mineral oil/glycerol mixture. The NP specimens were fixed in formalin (10%), dehydrated through alcohol passages, and directly immersed in a 1:1 mixture of mineral oil and glycerol, under vacuum (to degas the tissue and aid penetration) for 2 hours at room temperature, without having undergone paraffin embedding. The DP specimens were first processed as normal for histopathology, being fixed in formalin, dehydrated, then embedded in paraffin wax. Then the block was deparaffinized by first melting the block at 65° C, then using xylene and alcohol passages, and infiltrated with a 1:1 mineral oil and glycerol mixture under vacuum for 2 hours at room temperature. Lungs were inflated before fixation to preserve alveolar structure.

Imaging was performed with a home-built multiphoton laser scanning microscope, with ~200 fs optical pulses supplied by a Ti:sapphire oscillator (Spectra Physics Tsunami) operating at 810 nm. We used a 40x 0.8 NA water immersion objective (for its long working distance), and placed a coverslip on top of the intact specimen to provide a barrier between the oil/glycerol mixture and the immersion water column (though in principal, an objective designed for oil/glycerol immersion would improve our results). Optical power, unless otherwise specified, was approximately 35 mW. Fluorescence is directed by a dichroic mirror

#174845 - $15.00 USD Received 23 Aug 2012; revised 28 Sep 2012; accepted 1 Oct 2012; published 3 Oct 2012

(680 nm long-pass) to a photomultiplier tube (Hamamatsu, R3896, with a 600 nm short-pass filter (Thorlabs FES0600) and BG-39 glass to reject residual excitation light. This setup collects second-harmonic light and multiphoton autofluorescence simultaneously, in the same channel. Imaging depth is controlled by raising and lowering the microscope objective. For each organ, we acquired a z stack, 300 μm deep, with 3 μm steps, 4.9 μs pixel dwell time, 512x512 pixels, for an approximately 260 μm lateral field of view (FOV), unless otherwise specified. The organs were imaged with their outer surface in contact with the coverslip—no cutting or sectioning was performed.

3. Results

Images of each organ at selected depths are shown in Figs. 1-6, along with a profile of average signal intensity with respect to depth. The depth profiles for each image stack were calculated for a 32 × 32 μm region of interest, selected to avoid surface irregularities. The displayed image brightness is normalized so that black pixels are 0 (no signal), and white pixels are four standard deviations above the mean pixel brightness. Each image shown is a 130 × 130 μm FOV; the full 260 × 260 μm FOV for the top 100 μm of each stack is shown in Media 1-12. Photobleaching was observed with repeated imaging.

In the kidney, Fig. 1, the convoluted tubules are apparent in both NP and DP tissue preparations. The visibility of cells and nuclei is comparable between NP and DP. In the top layers of the DP z stack, blood cells can be seen in the peritubular capillaries. We were able to image slightly deeper into the DP specimen.

In the liver, Fig. 2, hepatocytes with grainy cytoplasm and dark nuclei are clear in the NP, but not the DP samples. However, gross architectural features such as sinusoids and hepatic arteries can be observed in both. Imaging depth appears comparable, but the DP cells appear damaged.

In the spleen, Fig. 3, it is difficult to discern any difference between white and red pulp, though the structure in the NP image stack suggests that a marginal sinus separating white and red pulp is in view. The NP images are slightly clearer than DP, though signal falloff with respect to depth is comparable.

In the heart, Fig. 4, striation pattern is from second-harmonic generated in myosin [22], the nuclei appear dark. We observe somewhat better imaging depth and clearer images in NP samples. Microvasculature, including blood cells, can be observed in the full z stack movies (online).

In the lung, Fig. 5, the alveolar structure is clear in both NP and DP tissue. The non-monotonic features in the decay curve results from the large regions devoid of tissue.

Finally, in the brain, Fig. 6, the greatest imaging depth was achieved—in excess of 250 μm in both NP and DP preparations. These images suggest that the transition between the molecular and granular layers is more prominent in NP specimen than in DP, while microvasculature was more visible in the DP specimen. Nuclei, however, are not visible in either preparation.

Volume imaging

Figure 7 shows a 3D volume rendering of a 260 × 260 × 65 μm section of a lung (acquired as a z stack with 0.5 μm z-step, rendered with Avizo; an exponential correction factor was applied to normalize the brightness of each slice). Clearing agents like Sca*l*e and BABB make tissue fragile [8,23], potentially posing a challenge for delicate tissues. In our method using oil and glycerol, we do not observe differences in handling properties between NP and DP samples.

#174845 - $15.00 USD Received 23 Aug 2012; revised 28 Sep 2012; accepted 1 Oct 2012; published 3 Oct 2012

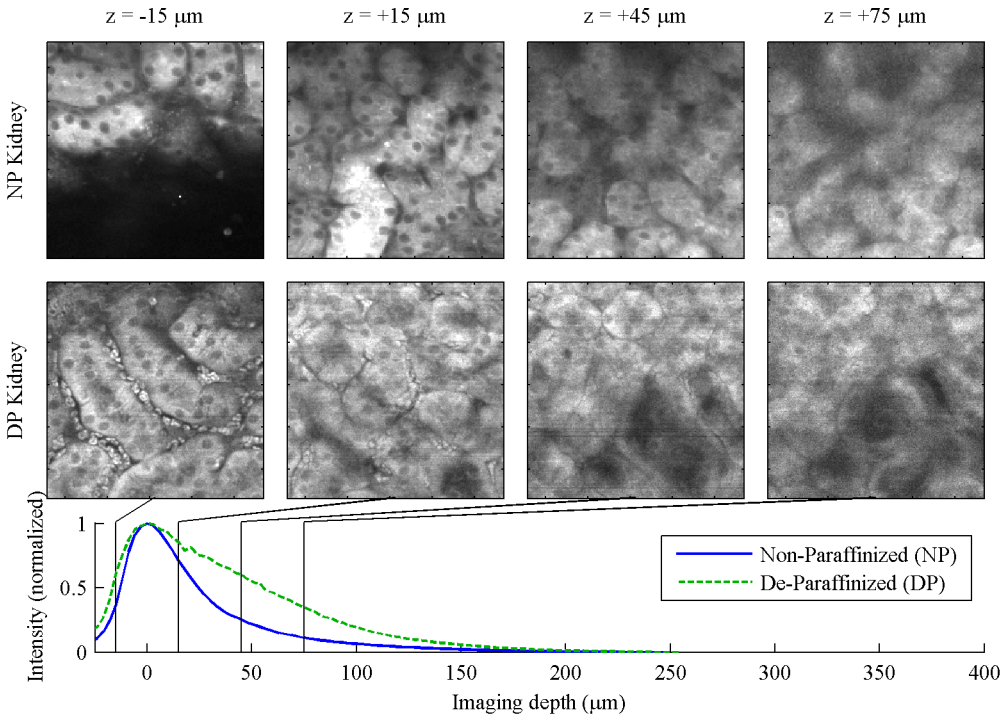

Fig. 1. Kidney, 130 μm FOV. (NP image acquired with 256 x 256 pixel resolution for the 260 μm field of view) For full 260 μm FOV, see Media 1 and Media 2.

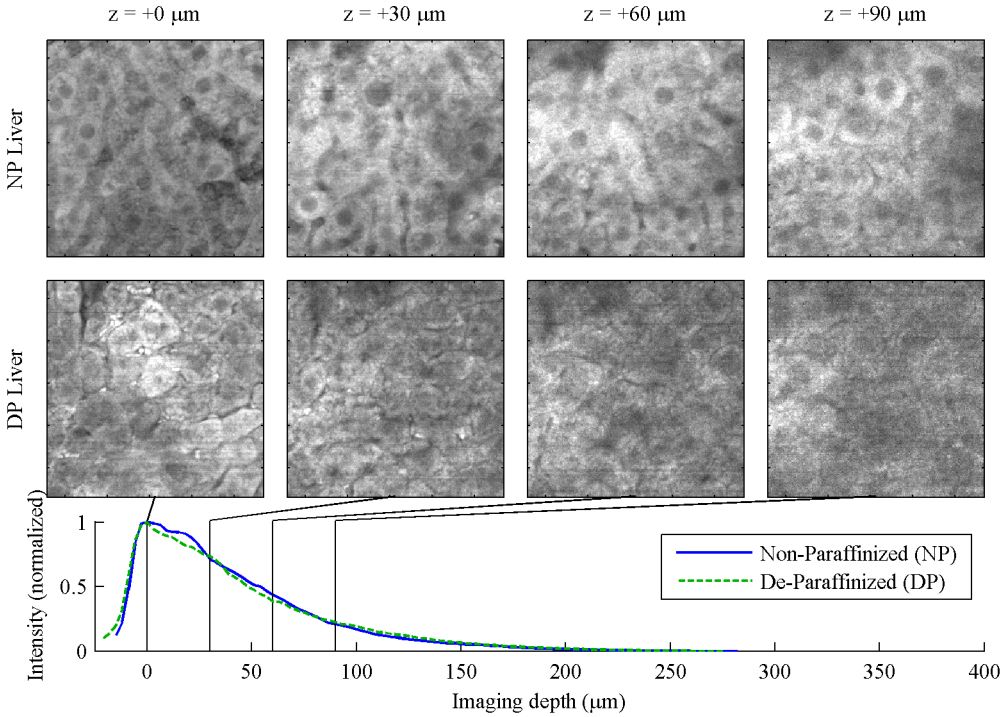

Fig. 2. Liver, 130 μm FOV. For full 260 μm FOV, see Media 3 and Media 4.

#174845 - $15.00 USD Received 23 Aug 2012; revised 28 Sep 2012; accepted 1 Oct 2012; published 3 Oct 2012

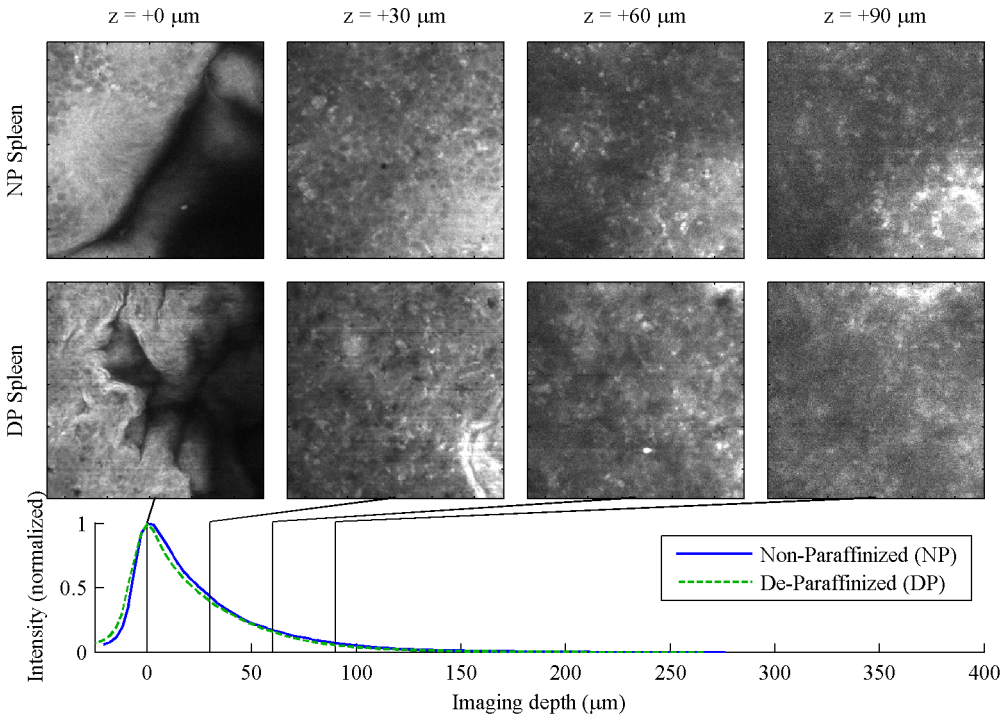

Fig. 3. Spleen, 130 μm FOV. For full 260 μm FOV, see Media 5 and Media 6.

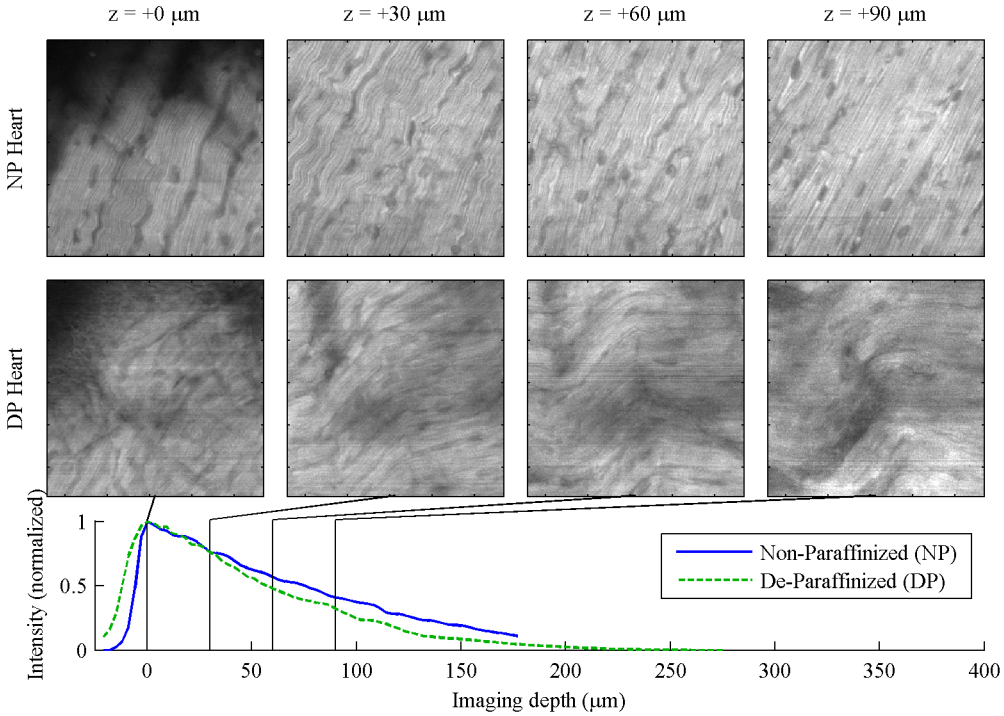

Fig. 4. Heart, 130 μm FOV. For full 260 μm FOV, see Media 7 and Media 8.

#174845 - $15.00 USD Received 23 Aug 2012; revised 28 Sep 2012; accepted 1 Oct 2012; published 3 Oct 2012

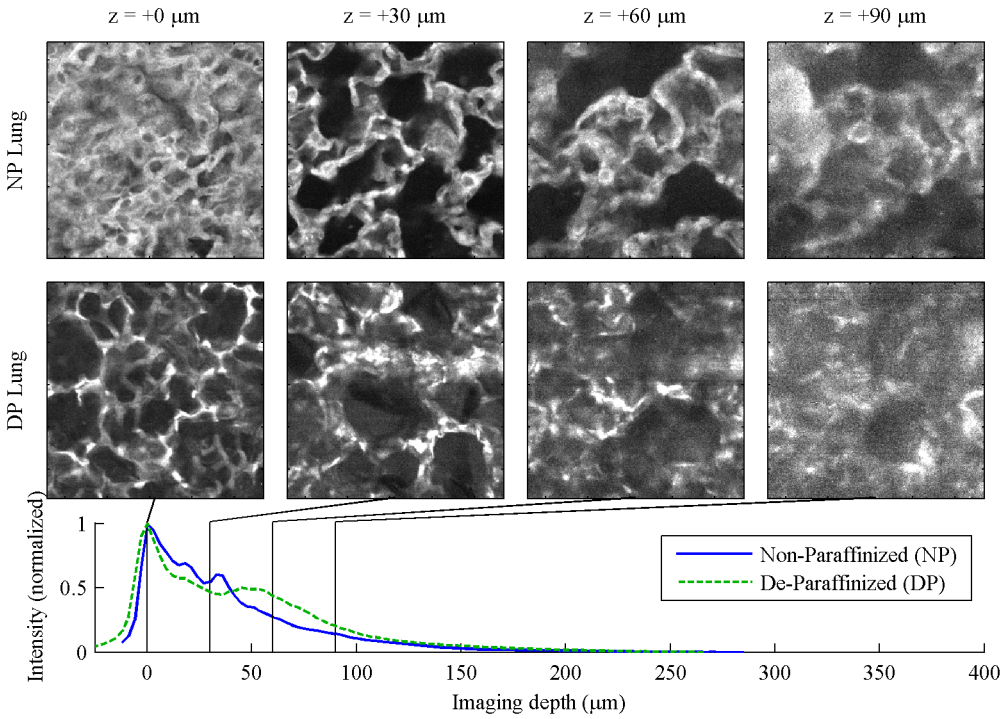

Fig. 5. Lung, 130 μm FOV. For full 260 μm FOV, see Media 9 and Media 10.

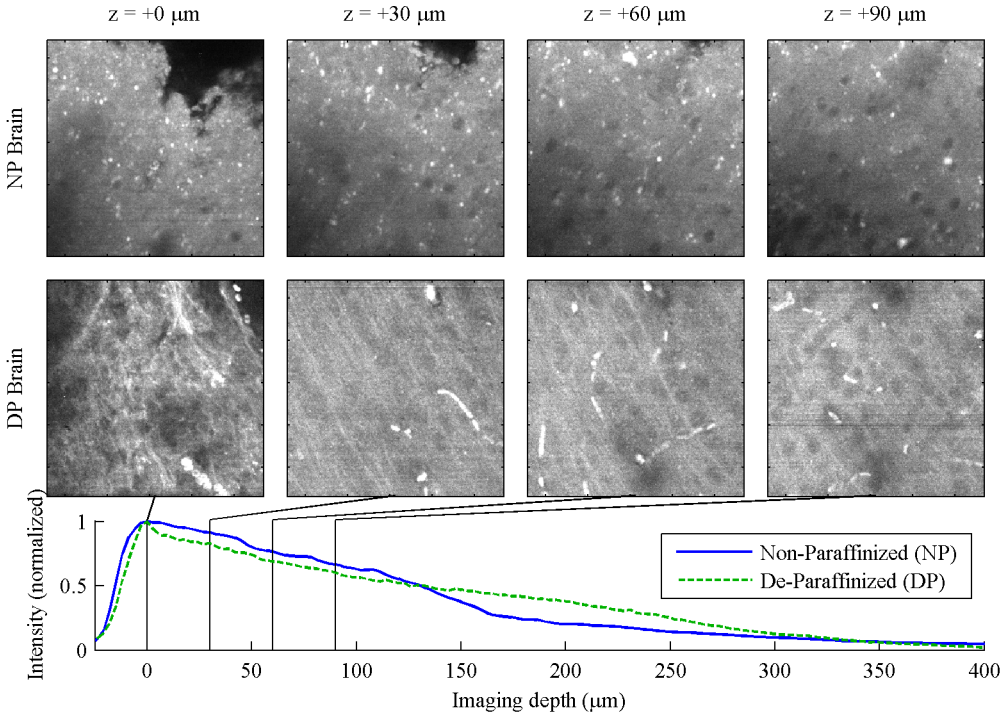

Fig. 6. Brain, 130 μm FOV. For full 260 μm FOV, see Media 11 and Media 12.

#174845 - $15.00 USD Received 23 Aug 2012; revised 28 Sep 2012; accepted 1 Oct 2012; published 3 Oct 2012

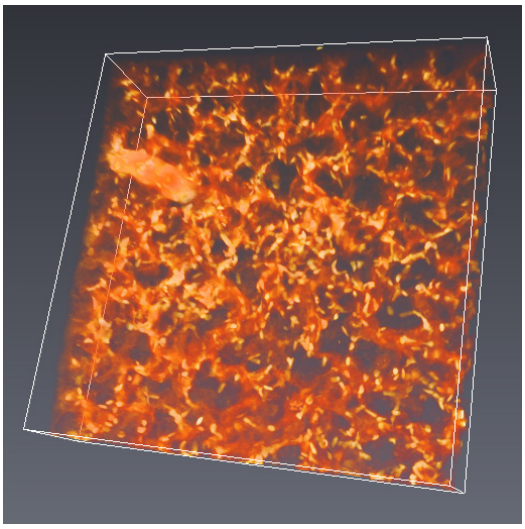

Fig. 7. Volume rendering of a 260 × 260 × 65 μm section of lung.

4. Discussion and conclusions

The contrast in these images is provided by multiphoton autofluorescence and second harmonic generation. Though both have been previously observed from fixed, cleared tissue [14], the observations here are the first to be reported from intact tissue that had been embedded in paraffin. The autofluorescence intensity in these specimens was significantly brighter than our previous experience with live tissue [24,25], leading us to attribute the source of autofluorescence not to intrinsic biological fluorophores, but to a byproduct of formalin fixation [26,27]. In this sense, the fixation process itself serves as a useful biological stain. The NP images were generally of higher quality than the DP images (likely a result of damage by the heating and cooling necessary for paraffin embedding [28]). In contrast to autofluorescence, SHG is not attributed to the fixative and is preserved during clearing (glycerol has been observed to dissociate collagen in fresh tissue [29], but the formaldehyde cross-linking process likely protects collagen from this effect in fixed tissue). We have observed SHG in the heart muscle, where it originates primarily from myosin (Fig. 4). We have also observed SHG from collagen both in NP and DP skin specimens (data not shown; the heterogeneity of the tissue makes it hard to compare the depth profile between non-paraffinized and de-paraffinized samples). It is important to point out that the reduced scattering loss through the index matching mechanism offers the same benefits for other imaging contrasts, such as transient absorption microscopy [30].

The achievable imaging depth might be improved by optimizing the oil:glycerol ratio and clearing time [19] or exploring other fluids [12,13]. Further gains can be achieved with instrumentation modifications such as spatio-temporal focusing [31] or spatial overlap modulation [32]. Also, the use of longer wavelengths can improve imaging depth [33] (though fluorescence is very sensitive to wavelength, several nonlinear contrast mechanisms are able to operate at arbitrary wavelengths, such as harmonic generation [34], four wave mixing [35], and nonlinear phase [36,37]).

The primary significance of our findings is the demonstration that multiphoton imaging can be employed on specimens stored in paraffin blocks, enabling retrospective studies. With minimal sample preparation, this technique enables easily accessible 3D histology on existing tissue archives. This ability could offer additional benefits to pathology. For example, if ambiguities arise from tissue processing (due to folding or unfavorable section selection), they could be resolved by 3D reconstruction. Though the oil/glycerol mixture cannot rival Sca*l*e or BABB clearing in terms of penetration depth, it offers other advantages: the technique here

#174845 - $15.00 USD Received 23 Aug 2012; revised 28 Sep 2012; accepted 1 Oct 2012; published 3 Oct 2012

can be employed to deparaffinize and clear tissue without the risk of dissolving melanin; and the cleared specimens are not fragile. The application of new multiphoton imaging methods to archived medical specimens could provide new insight into disease progression and help refine diagnostic criteria for accurate early detection.

Acknowledgments

This study was funded by the Duke University and the NIH (grant no. 1RC1CA145105).

#174845 - $15.00 USD Received 23 Aug 2012; revised 28 Sep 2012; accepted 1 Oct 2012; published 3 Oct 2012